Journal of Power Sources 192 (2009) 719–723

Contents lists available at ScienceDirect

Journal of Power Sources

journal homepage: www.elsevier.com/locate/jpowsour

Short communication

Hydrothermal synthesis of Co_2SnO_4 nanocrystals as anode materials for Li-ion batteries

G. Wang, X.P. Gao*, P.W. Shen

Institute of New Energy Material Chemistry, Nankai University, Tianjin 300071, China

ARTICLE INFO

Article history:
Received 12 January 2009
Received in revised form 9 February 2009
Accepted 24 February 2009
Available online 9 March 2009

Keywords:
Co_2SnO_4
Spinel structure
Hydrothermal reaction
Anode
Li-ion batteries

ABSTRACT

Cubic spinel Co_2SnO_4 nanocrystals are successfully synthesized via a simple hydrothermal reaction in alkaline solution. The effect of alkaline concentration, hydrothermal temperature, and hydrothermal time on the structure and morphology of the resultant products were investigated based on X-ray diffraction (XRD), scanning electron microscopy (SEM) and transmission electron microscopy (TEM). It is demonstrated that pure Co_2SnO_4 nanocrystals with good crystallinity can be obtained in NaOH solution (2.0 M) at 240 °C for 48 h. The galvanostatic charge/discharge and cyclic voltammetry were conducted to measure the electrochemical performance of the Co_2SnO_4 nanocrystals. It is shown that Co_2SnO_4 nanocrystals exhibit good electrochemical activity with high reversible capacity (charge capacity) of 1088.8 mAh g^{-1} and good capacity retention as anode materials for Li-ion batteries, much better than that of bulk Co_2SnO_4 prepared by high temperature solid-state reaction.

1. Introduction

Tin-based oxides and cobalt-based oxides have attracted a considerable attention because of their potential application in Li-ion batteries [1,2]. The theoretical capacity of SnO_2 and CoO can reach 1494 and 715 mAh g^{-1}, respectively, so that tin- or cobalt-based oxides are likely to be the potential candidates of anode materials for Li-ion batteries [2,3]. It was also reported that nano-sized metal oxides exhibited good electrochemical performance on account of the larger specific area and higher reaction activity for Li-ion insertion/extraction [2,4–6]. In recent years, some ternary metal compounds, such as stannates of M_2SnO_4 (M = Zn and Co) [7–9], MCo_2O_4 (M = Zn, Cu, Fe and Ni) [10–15] and MFe_2O_4 (M = Zn, Co and Ni) [16,17], have been investigated as anode materials for Li-ion batteries. In these compounds, the oxidation and reduction processes are involved for transition metal oxides, and lithium alloying exists in the subsequent reaction process of the tin oxides. In particular, multi-electron reaction is dominant in the electrochemical reaction processes of these compounds, leading to higher electrochemical capacity.

Cubic spinel Co_2SnO_4, where both Co and Sn are electrochemical active metals with respect to lithium, is an attractive anode material for lithium-ion batteries. Co_2SnO_4 with single phase structure is conventionally prepared from solid-state reaction at high temperature. Usually, Co_2SnO_4 samples, prepared by conventional solid-state reaction, show poor cycle stability due to large particle size and broad particle size distribution [7]. Hydrothermal method has been proved to be an adaptable way to prepare pure, uniform and well-crystallized products. Therefore, it can be a viable approach to synthesize Co_2SnO_4 powders by manipulating the synthesis conditions to achieve superior anode materials for Li-ion batteries.

In the present work, we report the synthesis of spinel Co_2SnO_4 via a facile hydrothermal pathway, and electrochemical properties of the as-prepared products as anode material were investigated.

2. Experimental

2.1. Preparation and characterization

Co_2SnO_4 nanocrystals (denoted as HT-Co_2SnO_4) were synthesized through a hydrothermal treatment in alkaline solution using $CoCl_2{\cdot}6H_2O$ and $SnCl_4{\cdot}5H_2O$ as raw materials. All the reagents were analytically pure, commercially available, and used without further purification. Firstly, $CoCl_2{\cdot}6H_2O$ and $SnCl_4{\cdot}5H_2O$ were dissolved into distilled water to form two transparent solutions. The two solutions were mixed together and then NaOH solutions (as mineralizer) with different concentrations were dropped into the Co–Sn mixture solution under magnetic stirring. The final mixture was fixed with concentrations of [Co] and [Sn] at 0.05 M and 0.025 M, respectively. The mixture was then transferred into a PTFE-lined stainless autoclave and kept at 150–240 °C for different time. After cooling down to ambient temperature, the resulting precipitates were collected by centrifugation, washed with distilled water and

* Corresponding author. Tel.: +86 22 23500876; fax: +86 22 23500876.
E-mail address: xpgao@nankai.edu.cn (X.P. Gao).

0378-7753/$ – see front matter © 2009 Elsevier B.V. All rights reserved.
doi:10.1016/j.jpowsour.2009.02.074

ethanol thoroughly, and finally dried in an electric oven at 120 °C for 12 h. The parameters of the hydrothermal reaction, such as the NaOH concentration, the hydrothermal temperature and the hydrothermal time, were investigated in order to understand the growth mechanism of the Co_2SnO_4 nanocrystalline. For comparison, Co_2SnO_4 bulk particles (denoted as SS-Co_2SnO_4) were also prepared by mixing Co_3O_4 and SnO_2 powders in a molar ratio of 2:3 and then calcined at 1200 °C, according to the high temperature solid-state reaction reported previously [8].

Crystallographic structure of the prepared samples was characterized by X-ray diffraction (XRD, Rigaku D/max-2500) using Cu Kα (λ = 1.5406 Å) radiation. The morphology and microstructure of the as-synthesized samples were measured with scanning electron microscope (SEM, Hitachi 3500N) and transmission electron microscope (TEM, FEI Tecnai 20).

2.2. Electrochemical measurements

The working electrodes were fabricated by mixing the active materials, acetylene black and polytetrafluoroethylene (PTFE) at the weight ratio of 60:20:20 into paste, then by roll pressing the paste into an electrode film, and finally by pressing the film onto a Cu foil current collector. The working electrodes were dried at 80 °C for 12 h in vacuum. A Li metal foil was used as the counter and reference electrode. The electrolyte was 1 M $LiPF_6$ in a mixture of ethylene carbonate (EC), propylene carbonate (PC), and dimethyl carbonate (DMC). The volume ratio of EC:PC:DMC in the mixture was 1:1:1. The cells were assembled in an atmosphere of high-purity argon in a glove box. Discharge–charge measurements of the cells were carried out with the potential range of 0.005 and 3.0 V (vs. Li^+/Li) using a LAND-CT2001A instrument. Cyclic voltammograms (CVs) experiment was carried out with a potential range of 0.005–3.0 V (vs. Li^+/Li) at a scan rate of 0.1 mV s^{-1} using a CHI 600A potentiostat at room temperature.

3. Results and discussion

Fig. 1 shows XRD patterns of the hydrothermally derived samples at 240 °C for 48 h in different alkaline concentrations. It is well-known that mineralizers such as MOH (M = Na, K, and Li) played a critical factor in the hydrothermal process of oxide electrode materials [9,18,19]. Without NaOH in the solution, only tetragonal phase of SnO_2 (JCPDS 41-1445) is formed due to the stronger hydrolysis effect of Sn^{4+} ions. When NaOH concentration increases to 1.0 M, a mixture of SnO_2, CoO with cubic structure (JCPDS 48-1719) and Co_2SnO_4 with cubic spinel structure (JCPDS 29-514) is obtained. The pure spinel Co_2SnO_4 with good crystallinity can be detected at 2.0 M NaOH solution. However, the hexagonal β-$Co(OH)_2$ (JCPDS 30-443), coexisted with spinel Co_2SnO_4, appears with further increasing the NaOH concentration to 3.0 M. In particular, both β-$Co(OH)_2$ and CoO exist at NaOH concentration of 4.0 M due to the formation of dissolved $Sn(OH)_6^{2-}$ in concentrated NaOH solution. The hydrated Co/Sn hydroxide precursor is a primary product before hydrothermal reaction. In the hydrothermal synthesis, alkaline concentration is effective for well-controlled growth of as-prepared metal oxides or compounds with desired morphology, size and phase composition [6,9,20,21]. The concentrated NaOH solution usually results in the partial or complete dissolution of the constituent element (Sn) formed by the complexation. While, individual oxides (SnO_2 and CoO) coexist with the desired compound (Co_2SnO_4) due to the weak driving force for the formation of stable spinel Co_2SnO_4 originated from the inherent crystal structure in lower NaOH concentration during the hydrothermal conversion process. Here, the optimal NaOH concentration is 2.0 M to obtain pure spinel Co_2SnO_4 with good crystallinity.

The effect of hydrothermal temperature on the formation of crystalline Co_2SnO_4 is observed from XRD patterns in Fig. 2. When the hydrothermal temperature is kept at 150 °C, a mixture of hexagonal β-$Co(OH)_2$ and cubic $Co(Sn(OH)_6)$ (JCPDS 74-365) is presented. With increasing hydrothermal temperature to 180–200 °C, the hydrothermal products mainly consists of β-$Co(OH)_2$, $Co(Sn(OH)_6)$ and $CoSnO_3$ (JCPDS 28-1236). At hydrothermal temperature of 220 °C, a trace of Co_2SnO_4 can be found with the main phase of $CoSnO_3$. Finally, the pure cubic spinel Co_2SnO_4 with good crystallinity is obtained at the temperature of 240 °C. It indicates that pure Co_2SnO_4 can be directly synthesized via the hydrothermal reaction when the temperature is high enough. The coexistence of $CoSnO_3$ and Co_2SnO_4 at 220 °C suggests that Co_2SnO_4 is formed, either directly nucleated from the synthesis solution or indirectly transformed from the $CoSnO_3$. Obviously, the reaction temperature is important in determining the phases of the resultant products.

XRD patterns of the samples synthesized at 240 °C with different hydrothermal time are shown in Fig. 3. When the hydrothermal time is only 1 h, the diffraction peaks of the cubic spinel Co_2SnO_4 appear with the hexagonal β-$Co(OH)_2$. With increasing hydrother-

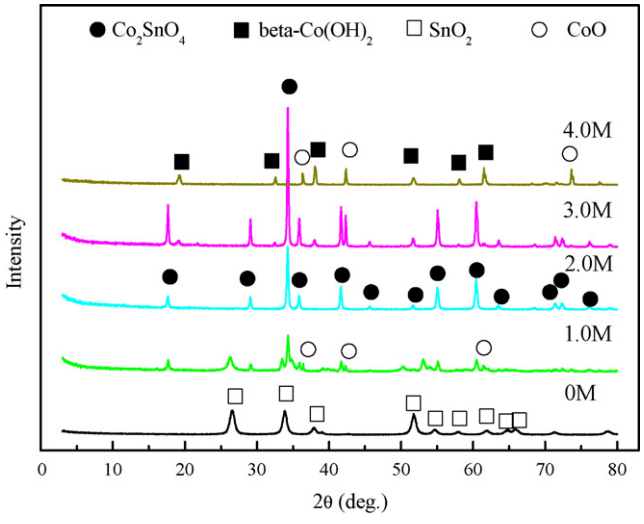

Fig. 1. XRD patterns of the as-prepared samples at 240 °C for 48 h, using NaOH concentrations of (a) 0 M, (b) 1.0 M, (c) 2.0 M, (d) 3.0 M, and (e) 4.0 M.

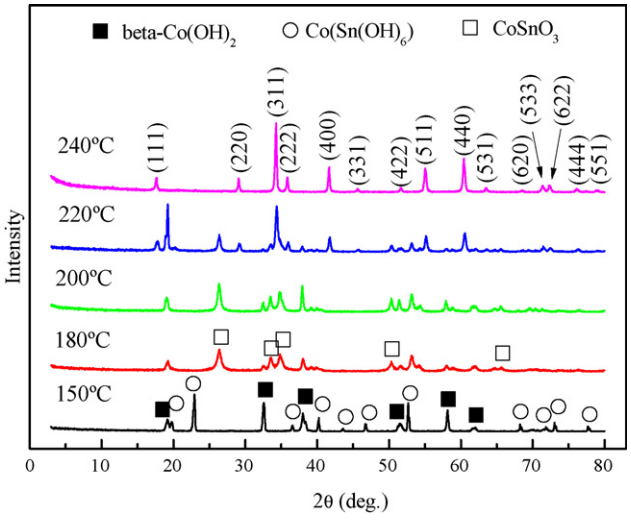

Fig. 2. XRD patterns of the as-prepared samples at different hydrothermal temperature for 48 h in 2.0 M NaOH solution.

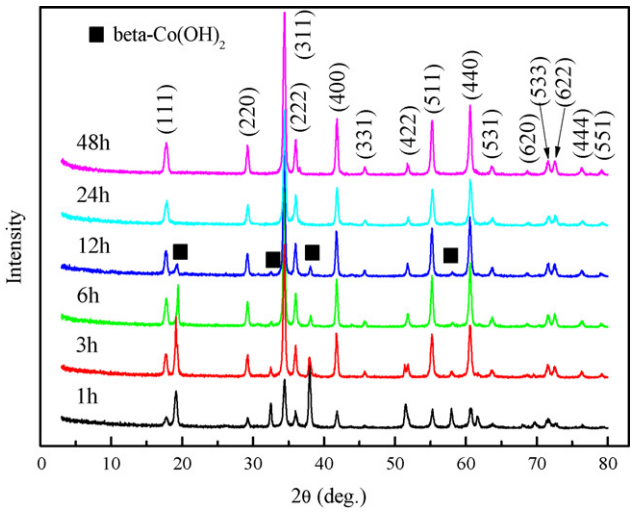

Fig. 3. XRD patterns of the as-prepared samples at different hydrothermal time at 240 °C in 2.0 M NaOH solution.

mal time, the diffraction peaks of hexagonal phase β-$Co(OH)_2$ disappear gradually. All the diffraction peaks in the patterns could be indexed to the pure cubic spinel Co_2SnO_4 after 24 h. Clearly, longer hydrothermal time is in favor of the structure transformation to the Co_2SnO_4 phase. After hydrothermal reaction for 48 h, the more perfect crystallization of the sample is presented. It is noted that the $CoSnO_3$ phase does not appear at 240 °C.

Fig. 4 displays SEM images of the products synthesized via hydrothermal reaction and high temperature solid-state reaction. The spherical products obtained by the hydrothermal treatment at 240 °C for 48 h with 2.0 M NaOH concentration are uniform with a particle size less than 100 nm (Fig. 4a). Moreover, nano-size particles with an average size of 80–120 nm are clearly seen from TEM images in Fig. 5. The calculated interference fringe spacing from the intensity line profile as inserted in HRTEM was about 0.49 nm, consistent with the interplanar distance of (1 1 1) planes of cubic spinel Co_2SnO_4 in the XRD pattern. Therefore, we can conclude that the hydrothermal reaction at relatively low temperature of 240 °C is beneficial to the formation of nano-sized and well-crystallined Co_2SnO_4. However, Co_2SnO_4 particles prepared by solid-state reaction at high temperature have irregular shapes and broad particle size distribution (Fig. 4b). In particular, some smaller particles (about 100 nm) coexist with larger particles (1–2 μm).

Fig. 6 shows initial discharge–charge curves of the as-prepared Co_2SnO_4 prepared by hydrothermal treatment (HT-Co_2SnO_4) and the high temperature solid-state reaction (SS-Co_2SnO_4) at a current density of 30 mA g^{-1}. The two electrodes exhibit similar profile in the initial discharge curves with an extended potential plateaus at around 0.9 V (vs. Li^+/Li), followed by two sloping potentials at about 0.5 V and below 0.3 V. It is obvious that reversible capacity (charge capacity) and charge potential profile in the second cycle are almost identical to that in the first cycle, indicating a good reversibility of the HT-Co_2SnO_4 sample. On contrast, a poor reversibility is observed for the SS-Co_2SnO_4 sample. Analogous to other binary and ternary tin oxides [2,7–9], the structure destruction and the formation of Co- and Sn-nano-particles in an amorphous matrix of Li_2O are involved in the initial discharge reaction process (Eq. (1)). The subsequent reaction of Li with Sn-metal results in the formation of $Li_{4.4}Sn$ alloy (Eq. (2)).

$$Co_2SnO_4 + 8Li \leftrightarrow 2Co + 4Li_2O + Sn \quad (1)$$

$$Sn + 4.4Li \leftrightarrow Li_{4.4}Sn \quad (2)$$

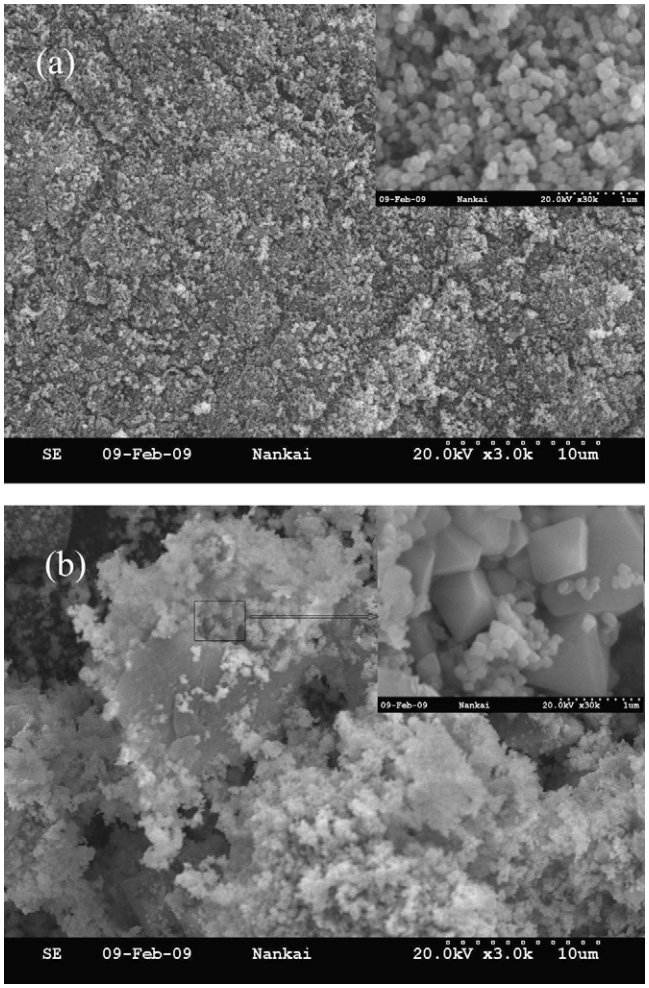

Fig. 4. SEM images of the products synthesized via hydrothermal reaction (a) and high temperature solid-state reaction (b). SEM images at high magnification are inserted.

The initial overall discharge capacities for HT-Co_2SnO_4 and SS-Co_2SnO_4 at a current density of 30 mA g^{-1} are 1533.1 and 1400.9 mAh g^{-1}, respectively. Correspondingly, 17.2 and 15.7 mol/Li are consumed in the initial discharge reaction for HT-Co_2SnO_4 and SS-Co_2SnO_4, respectively, whereas the theoretical value is only 12.4 mol/Li according to Eqs. (1) and (2). Thus, the excess of Li consumed in the initial discharge process may be ascribed to the decomposition of the electrolyte, and subsequent formation of an organic layer on the surface of the particles and carbon additive, as well as a trace amount water in the assembled cells [9,22,23]. It seems that the HT-Co_2SnO_4 sample consumes more Li than SS-Co_2SnO_4, attributed to their small particle size of HT-Co_2SnO_4. The initial charge capacities are 1088.8 mAh g^{-1} (12.2 mol of Li) for HT-Co_2SnO_4, and 906.1 mAh g^{-1} (10.2 mol of Li) for SS-Co_2SnO_4 and their initial coulombic efficiency are 71% and 64.5%, respectively. The high reversible capacities (charge capacities) with >4.4 Li extraction reveal that the reversible contribution not only come from above reactions (Eq. (2)), but also be related to other reactions. It is known that tin oxidation [3,24] take place at about 1.5 V (vs. Li^+/Li) and cobalt oxidation [25,26] commonly occurs at about 2.0 V (vs. Li^+/Li) as followed:

$$Sn + 2Li_2O \leftrightarrow SnO_2 + 4Li \quad (3)$$

$$Co + Li_2O \leftrightarrow CoO + 2Li \quad (4)$$

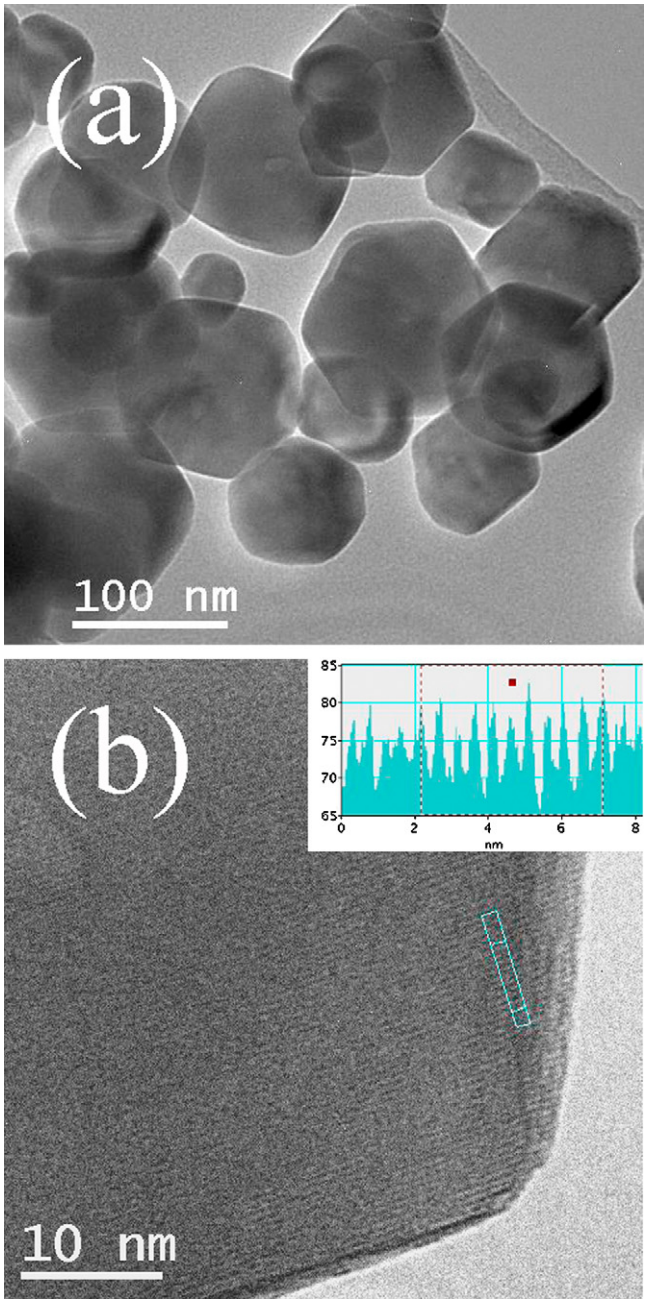

Fig. 5. TEM images of Co_2SnO_4 synthesized via hydrothermal reaction. The intensity line profile for a selected area of the Co_2SnO_4 nanocrystal is inserted in (b).

The measured reversible results match well with the theoretical capacities, derived from the maximum uptake of 12.4 Li/Co_2SnO_4 according to Eqs. (2), (3) and (4). Thus, both cobalt and tin participate in the reversible redox processes during electrochemical cycling.

The cycle performance of the as-prepared HT-Co_2SnO_4 and SS-Co_2SnO_4 electrodes at 30 mA g^{-1} is indicated in Fig. 7. The discharge capacity of HT-Co_2SnO_4 is 555.9 mAh g^{-1} after 50 cycles and the capacity retention is 50.3%, much higher than that of SS-Co_2SnO_4 (112.8 mAh g^{-1} with the capacity retention of only 12.2% after 50 cycles). Actually, the particle size, morphology, and crystallinity have a great influence on the cyclic performance of transition metal oxides as anode materials [6,9,27,28]. It is understood that the larger crystallites after discharging will be poorly interconnected to facilitate charge transfer leading to reduced cycle performance, in

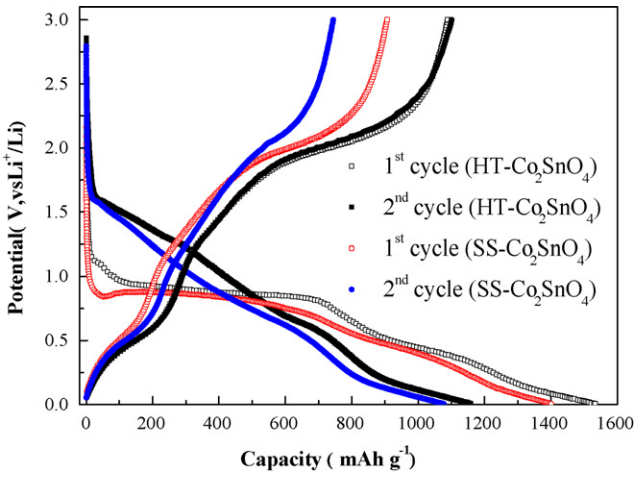

Fig. 6. The initial discharge–charge curves of HT-Co_2SnO_4 and SS-Co_2SnO_4 at 30 mA g^{-1}.

accordance with the observations of larger SnO_2 crystallites with poor cycling performance [29,30]. Moreover, smaller crystallites with larger surface area may accommodate the stress caused by volume change during repeatedly charge/discharge cycling, resulting in improved cyclic performance. However, it should be noted that the relatively low retention for HT-Co_2SnO_4 after 50 cycles is still observed, which has a negative impact on its potential application. Further improving the cycle stability is necessary for HT-Co_2SnO_4.

Fig. 8 shows typical cyclic voltammograms (CVs) of the HT-Co_2SnO_4 and SS-Co_2SnO_4 electrodes. The CVs of the first anodic and cathodic processes for the two electrodes have similar profile. A clear reduction peak in the cathodic process at ~0.6 V (vs. Li^+/Li) with an onset at ~1.0 V (vs. Li^+/Li) in the first cycle can be attributed to the multi-step electrochemical lithium reaction process with the decomposition of Co_2SnO_4 into Co and Sn, and the formation of amorphous Li_2O and the SEI film [11,31–35]. A peak located at about 0.25 V (vs. Li^+/Li) is attributed to the formation of Li–Sn alloys [31,36]. Three oxidation peaks at 0.6, 1.3 and 2.1 V are shown in the first anodic process up to 3.0 V (vs. Li^+/Li), corresponding to the de-alloying process (~0.6 V) [3,31,37], the re-oxidation reaction of tin (~1.3 V) [3,24,37] and the re-oxidation reaction of cobalt atoms (~2.1 V) [25,26], respectively. In the second and subsequent cycles, the redox couple, indexed as a/a′, corresponds to the alloying/de-alloying process of Li_xSn. Other two redox couples, indexed as b/b′ at 0.7/1.3 V and c/c′ at 1.3/2.1 V, appear due to the

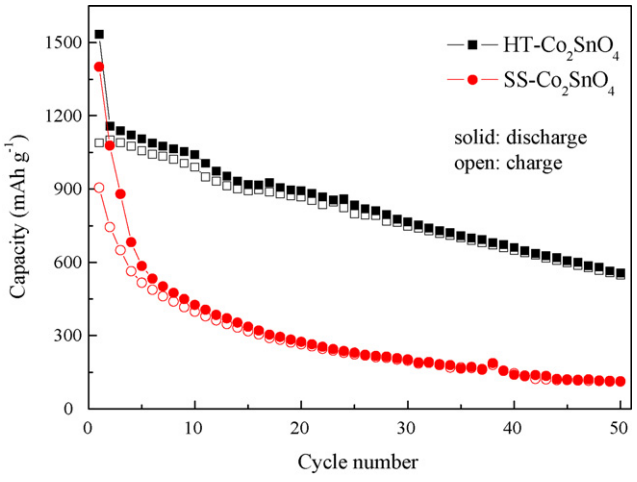

Fig. 7. Cycle performance of HT-Co_2SnO_4 and SS-Co_2SnO_4 at 30 mA g^{-1}.

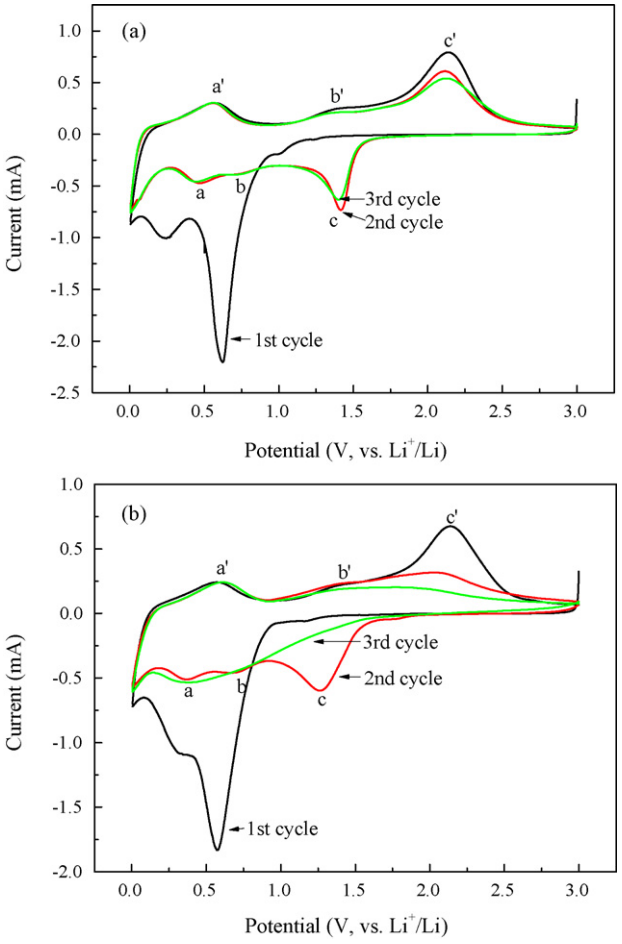

Fig. 8. Cyclic voltammograms of HT-Co_2SnO_4 (a) and SS-Co_2SnO_4 (b) at a scan rate of 0.1 mV s^{-1} in the potential range 0.005–3.0 V (vs. Li^+/Li).

reversible reactions to some extent based on Eqs. (3) and (4). Higher potentials than 1.0 V as driving force may result in the formation and deformation of Li_2O [38]. However, for the SS-Co_2SnO_4 electrode, the redox couple of c/c′ nearly disappear after the first anodic and cathodic processes, indicating that the cobalt is hardly reduced in subsequent cycles for SS-Co_2SnO_4. This is in agreement with the poor cycle stability of SS-Co_2SnO_4 as shown above. The poor capability for the re-oxidation of Co on non-conductive Li_2O matrix is related to longer diffusion length for larger crystallites. The result is helpful to explore new nanostructure oxides or compounds with high capacity as anode materials for lithium-ion batteries.

4. Conclusion

In summary, cubic spinel Co_2SnO_4 nanocrystals were successfully synthesized via a simple hydrothermal reaction in alkaline solution. The alkaline concentration, hydrothermal temperature and hydrothermal time play important roles in the formation of Co_2SnO_4 nanocrystals. Pure Co_2SnO_4 with good crystallinity can be obtained after hydrothermal reaction in NaOH solution (2.0 M) at 240 °C for 48 h. The electrochemical results show that the high reversible capacity (charge capacity) of 1088.8 mAh g^{-1} is achieved at 30 mA g^{-1} in the potential range of 0.005–3.0 V. The capacity retention is 50.3% after 50 cycles, much higher than that of bulk Co_2SnO_4 prepared by high temperature solid-state reaction.

Acknowledgment

This work is supported by the 973 Program (2009CB220100), China.

References

[1] Y. Idota, T. Kubota, A. Matsufuji, Y. Maekawa, T. Miyasaka, Science 276 (1997) 1395.
[2] P. Poizot, S. Laruele, S. Grugeon, L. Dupont, J.M. Tarascon, Nature 407 (2000) 496.
[3] I.A. Courtney, J.R. Dahn, J. Electrochem. Soc. 144 (1997) 2943.
[4] J.M. Tarascon, M. Armand, Nature 414 (2001) 359.
[5] P.G. Bruce, B. Scrosati, J.M. Tarascon, Angew. Chem. Int. Ed. 47 (2008) 2930.
[6] X.P. Gao, J.L. Bao, G.L. Pan, H.Y. Zhu, P.X. Huang, F. Wu, D.Y. Song, J. Phys. Chem. B 108 (2004) 5547.
[7] P.A. Connor, J.T.S. Irvine, J. Power Sources 97–98 (2001) 223.
[8] P.A. Connor, J.T.S. Irvine, Electrochim. Acta 47 (2002) 2885.
[9] A. Rong, X.P. Gao, G.R. Li, T.Y. Yan, H.Y. Zhu, J.Q. Qu, D.Y. Song, J. Phys. Chem. B 110 (2006) 14754.
[10] C.C. Ai, M.C. Yin, C.W. Wang, J.T. Sun, J. Mater. Sci. 39 (2004) 1077.
[11] Y. Sharma, N. Sharma, G.V.S. Rao, B.V.R. Chowdari, J. Power Sources 173 (2007) 495.
[12] Y. Sharma, N. Sharma, G.V.S. Rao, B.V.R. Chowdari, Solid State Ionics 179 (2008) 587.
[13] Y.N. Nuli, P. Zhang, Z.P. Guo, H.K. Liu, J. Yang, Electrochem. Solid-State Lett. 11 (2008) A64.
[14] Y. Sharma, N. Sharma, G.V. Subba, B.V.R. Chowdari, Adv. Funct. Mater. 17 (2007) 2855.
[15] A.V. Chadwick, S.L.P. Savin, S. Fiddy, R. Alcantara, D.F. Lisbona, P. Lavela, G.F. Ortiz, J.L. Tirado, J. Phys. Chem. C 111 (2007) 4636.
[16] P. Lavela, J.L. Tirado, J. Power Sources 172 (2007) 379.
[17] Y. Sharma, N. Sharma, G.V.S. Rao, B.V.R. Chowdari, Electrochim. Acta 53 (2008) 2380.
[18] M. Tabuchi, Y. Nabeshima, M. Shikano, K. Ado, H. Kageyama, K. Tatsumi, J. Electrochem. Soc. 154 (2007) A638.
[19] Q. Liu, Y.X. Li, Z.L. Hu, D.L. Mao, C.K. Chang, F.Q. Huang, Electrochim. Acta 53 (2008) 7298.
[20] J. Li, Z. Zhou, L. Zhu, K. Xu, H. Tang, J. Phys. Chem. C 111 (2007) 16768.
[21] S.L. Zhong, J.M. Song, S. Zhang, H.B. Yao, A.W. Xu, W.T. Yao, S.H. Yu, J. Phys. Chem. C 112 (2008) 19916.
[22] N. Sharma, G.V. Subba Rao, B.V.R. Chowdari, J. Power Sources 159 (2006) 340.
[23] N. Sharma, J. Plevert, G.V. Subba-Rao, B.V.R. Chowdari, T.J. White, Chem. Mater. 17 (2005) 4700.
[24] R. Alcantara, F.J. Fernandez-Madrigal, C. Perez-Vicente, J.L. Tirado, J.C. Jumas, J. Olivier-Fourcade, Chem. Mater. 11 (1999) 2687.
[25] P. Poizot, S. Laurelle, S. Grugeon, L. Dupont, J.M. Tarascon, J. Power Sources 97–98 (2001) 235.
[26] H.C. Choi, S.Y. Lee, S.B. Kim, M.G. Kim, M.K. Lee, H.J. Shin, J.S. Lee, J. Phys. Chem. B 106 (2002) 9252.
[27] Y. Nuli, R. Zeng, P. Zhang, Z.P. Guo, H.K. Liu, J. Power Sources 184 (2008) 456.
[28] X.L. Wu, Y.G. Guo, L.J. Wan, C.W. Hu, J. Phys. Chem. C 112 (2008) 16824.
[29] W.F. Liu, X.J. Huang, Z.X. Wang, H. Li, L.Q. Chen, J. Electrochem. Soc. 145 (1998) 1.
[30] C. Kim, M. Noh, M. Choi, J. Cho, B. Park, Chem. Mater. 17 (2005) 3297.
[31] D. Aurbach, A. Nimberger, B. Markovsky, E. Levi, E. Sominski, A. Gedanken, Chem. Mater. 14 (2002) 4155.
[32] M. Marcinek, L.J. Hardwick, T.J. Richardson, X. Song, R. Kostecki, J. Power Sources 173 (2007) 965.
[33] C.C. Chang, S.J. Liu, J.J. Wu, C.H. Yang, J. Phys. Chem. C 111 (2007) 16423.
[34] C.Q. Zhang, J.P. Tu, X.H. Huang, Y.F. Yuan, S.F. Wang, F. Mao, J. Alloys Compd. 457 (2008) 81.
[35] P. Lavela, G.F. Ortiz, J.L. Tirado, E. Zhecheva, R. Stoyanova, S. Ivanova, J. Phys. Chem. C 111 (2007) 14238.
[36] M.Z. Xue, Z.W. Fu, Electrochem. Solid-State Lett. 9 (2006) A468.
[37] R. Alcantara, G.F. Ortiz, P. Lavela, J.L. Tirado, Electrochem. Commun. 8 (2006) 731.
[38] I.A. Courtney, J.R. Dahn, J. Electrochem. Soc. 144 (1997) 2045.